From seismic data to core data: an integrated approach to enhance reservoir characterization

JONNY HESTHAMMER[1] & HAAKON FOSSEN[2]

[1]*Statoil, N-5020 Bergen, Norway (e-mail: jonhe@statoil.no)*
[2]*Department of Geology, University of Bergen, Allegt. 41, N-5007 Bergen, Norway (e-mail: haakon.fossen@geol.uib.no)*

Abstract: Integrated structural analyses of seismic and various well data are necessary to optimize hydrocarbon reservoir characterization. However, there are many published examples from the oil and gas industry where single data types are analysed but not integrated. This may lead to erroneous interpretations and drainage strategies. As illustrated by an example from the area around well 34/10–B-12 in the North Sea Gullfaks Field, integrated structural interpretation should typically utilize all available seismic surveys, well log correlation data, dipmeter data and core data. Interpretation of seismic data helps in the understanding of large-scale structural and stratigraphic geometries. Time-lapse (4D) seismic helps to identify changes in reservoir properties caused by injection and production. Well log correlation data are used to document variations in zonation thickness caused by sedimentological or structural changes. Dipmeter data tie observations of bedding orientation from seismic data to subseismic scale. Core data represent the most detailed (millimetre to metre scale) data available and can yield information on rock properties as well as sedimentological and (micro)structural features. Small-scale deformation structures such as deformation bands and fractures can typically be identified and characterized. In addition, it is possible from unorientated cores to find the orientation of bedding and deformation structures. This information is compared to observations from dipmeter data, well log correlation data and seismic data to improve the interpretation.

Well 34/10–B-12 is a hanging wall injector near one of the large-scale faults in the Gullfaks Field. Several 3D seismic surveys are available from the area, as are standard well log data, dipmeter information and cores. Together, the data range from millimetre to kilometre with some overlap between the data types. Through integrated analysis, pitfalls such as interpreting any linear feature on timedip attribute maps as faults has been avoided. Also, a geometric relation between core-scale and seismic-scale faults has been established, and it has been possible to relate small-scale and large-scale structures in a model which is consistent with all the available data.

Deformed reservoirs require integrated use of all available sources of information rather than 'stand-alone' interpretation of the individual data types. However, for various reasons, the simple principle of integration is commonly neglected in the interpretation of oil and gas fields, potentially leading to serious misinterpretations and erroneous drainage strategies (Hesthammer *et al*. 2001). This paper demonstrates how the analysis and integration of seismic data, stratigraphic log correlation data, dipmeter data, production (pressure) data and core data give a comprehensive understanding of the reservoir characteristics in the area around one of the wells drilled in the Gullfaks Field, northern North Sea (Fig. 1).

The Gullfaks Field covers an area of *c*. 55 km^2, and contains more than 200 wells with information from more than 125 km of drilled reservoir rocks. Among the available well data are 34 km of dipmeter data and 6 km of core data. The field is structurally complex, but large amounts of well data have helped to outline the structural geology of the field (Fossen & Hesthammer 1998a). The Gullfaks Field is divided into three structural domains: a western domino-style fault system with easterly dipping faults and westerly dipping bedding; an eastern horst complex of elevated subhorizontal layering and steep faults; and a transitional accommodation zone (graben system) which is in part identified as a modified anticlinal fold structure (Fig. 1b). Total reserves amount to 319×10^6 standard m^3 of oil and some 30×10^9 standard m^3 of gas in the Jurassic Brent Group, the Cook and Statfjord Formation (Fm.) reservoirs (Fig. 2).

Well log correlation has identified 290 faults with displacements ranging from 4 m to more than 500 m. Many of these faults are also identified from dipmeter analyses. If the faults are

From: AMEEN, M. (ed.). *Fracture and In-Situ Characterization of Hydrocarbon Reservoirs*. Geological Society, London, Special Publications, 209, 39–54 0305–8719/••/$15.00

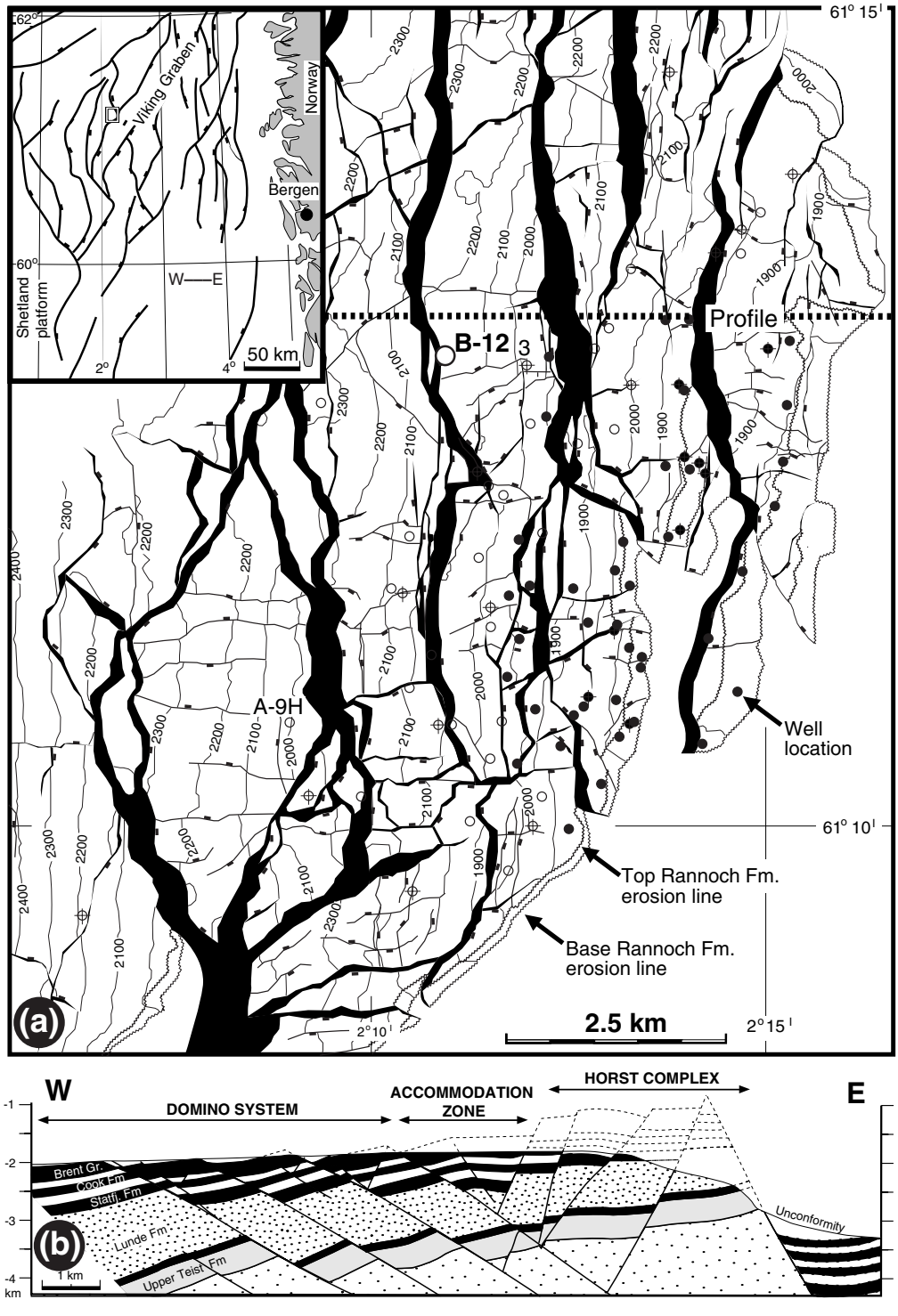

Fig. 1. (**a**) Structure map of the Rannoch Fm. in the Gullfaks Field; see inset map for location. (**b**) East–West profile through the three different structural domains; see (a) for location. Modified after Fossen & Hesthammer (1998a).

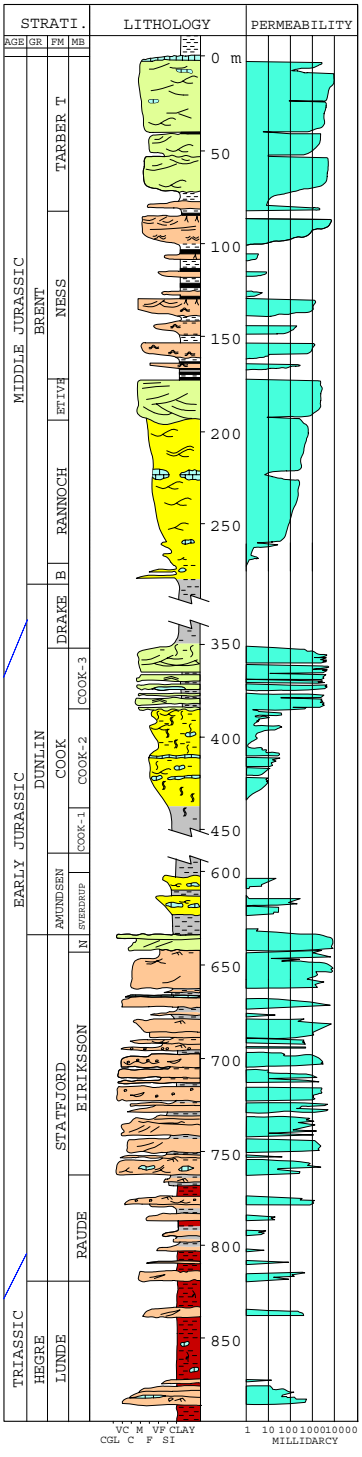

Fig. 2. Stratigraphic column for the Jurassic and Triassic reservoir units within the Gullfaks Field. Modified after Tollefsen *et al.* (1994).

associated with drag of bedding (which applies to more than 60% of all faults; Hesthammer & Fossen 1998), it is often possible to estimate the orientation of the faults. In addition, the width of the drag zones can be quantified. This can then be used for analyses of sealing potential of the faults. Comparison of faults identified from detailed well log correlation with seismic data demonstrates that only 25% of faults with displacement less than 30 m can be identified in the seismic data (Hesthammer & Fossen 2001). For faults with displacements that exceed 30 m, more than 67% of the faults can be observed on the seismic survey. This important observation can help the geologist to avoid overinterpreting seismic data as well as to identify the potential for structural interpretation.

Core analyses demonstrate that faults in the Gullfaks Field are associated with abundant deformation bands. Such zones of deformation bands are easily identified and quantified from fracture frequency diagrams. The deformation bands can reduce the permeability of the sandstones by up to three orders of magnitude (depending on the content of mica; Hesthammer 1999b; Hesthammer & Fossen 2001) and represent important barriers for fluid flow. Within the narrow fault zone, the deformation bands tend to become subparallel to the larger faults. Orientation analysis of deformation bands therefore also yields information on the orientation of the larger-scale faults. It is possible from unoriented cores to find the orientation of faults provided that the orientation of bedding is known.

Well 34/10–B-12

Well 34/10–B-12, which is an injector in the Middle Jurassic Tarbert Fm. (Fig. 2), is used in this example to demonstrate how seismic and well data can be integrated to enhance the structural understanding of an area. The well is located mainly in the hanging wall to two large-scale faults (Fig. 3) but penetrates the faults in the lower part of the well. In addition to seismic and standard well data, dipmeter and core data were collected for sedimentological and structural analyses.

Seismic data

Several seismic surveys have been collected over the Gullfaks Field. The reasons for collecting more than one survey is mainly related to improvements in data acquisition procedure. In addition, studies of time-lapse (4D) seismic lead to better oil recovery by identifying areas where

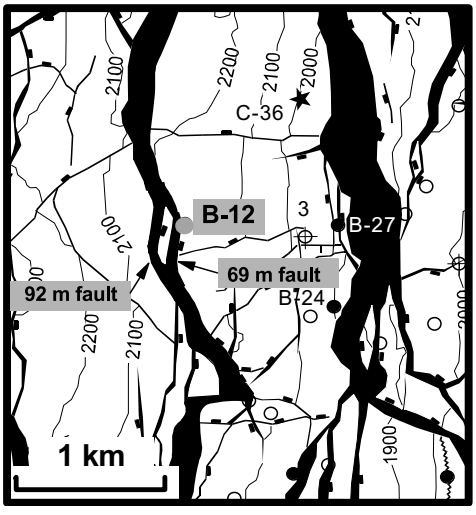

Fig. 3. Structure map of the Rannoch Fm. from the area around well 34/10–B-12. Two faults associated with 69 m and 92 m missing section, respectively, have been identified from well log correlation. Seismic data, dipmeter data and core data show that the faults dip 25–35° towards the ESE.

the oil has not been drained by existing producers. Once available, different seismic surveys may be combined to enhance data quality for structural interpretation (Hesthammer & Løkkebø 1997; Hesthammer 1999a).

As an example, Figure 4 shows two seismic profiles from where well 34/10–B-12 penetrates two main faults. Figure 4a is from the survey collected in 1985 (and reprocessed in 1992) whereas Figure 4b is from the 1996 survey. In general, the main faults and seismic reflections are better imaged in the oldest survey. This somewhat surprising observation is probably related to non-optimal acquisition geometries and processing procedures of the 1996 data.

Although two large-scale faults have been identified from well-log correlation, the faults are indistinguishable on the seismic data. This is due to the closeness of the two faults (located only 15 m apart). Within the hanging wall, bedding dip decreases somewhat towards the faults as a result of large-scale drag which is commonly observed within the domino system (Fossen & Hesthammer 1998*a*). The footwall does not display any gradual change in dip and thus

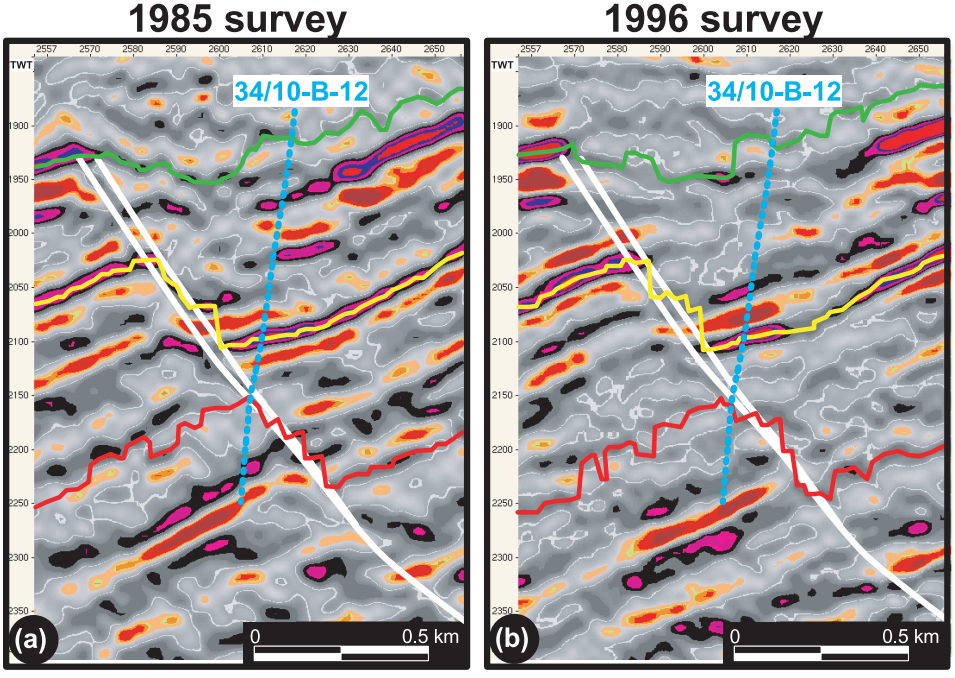

Fig. 4. (**a**) Seismic east–west profile from the area around well 34/10–B-12. The seismic data are from a 1985 survey that was reprocessed in 1992. A large-scale fault offsets the seismic reflections. Detailed well log correlation show that the fault actually consist of two faults associated with 69 m and 92 m missing section. The seismic resolution does not allow separation of the two faults. (**b**) Same as (a) but from a survey acquired in 1996. The fault is less obvious in this data set. In addition, the seismic reflections appear to be less continuous.

appears from seismic data to be unaffected by deformation.

Based on interpretation of the seismic reflections, several seismic attribute maps can be generated. For structural interpretation of the Gullfaks Field, the timedip map (Dalley *et al*. 1989; Hoetz & Watters 1992; Voggenreiter 1991) proved most useful. Figure 5a shows a timedip map of the intra-Ness Fm. (Fig. 2) reflection from the area around well 34/10–B-12. The map was created by snapping the interpretation to the nearest maximum and then calculating the derivative of the snapped horizon. Dark lines represent jumps in the interpretation that may be related to real features such as faults, or may be seismic artifacts caused by noise interference problems (Hesthammer & Fossen 1997*a*, *b*). The prominent dark centrelines are related to offset of the intra-Ness Fm. reflection caused by the main faults. The presence of two such distinct linear features may erroneously be interpreted to represent offset along the two main faults. To improve the visual impression of the attribute map along the fault, the interpreted horizon was interpolated across the faulted area prior to snapping. The linear features arise as the autotracked horizon attempts to follow the trace of the fault plane. Where the fault plane reflection is weak or absent, the autotracked horizon will tend to follow bedding plane reflections or multiples in a stepwise manner (Fig. 5c).

Within the footwall area to the main fault, several (curvi-)linear fault-like features are present. Whether these represent real faults or not cannot be determined from analyses of data from the 34/10–B-12 well alone. However, numerous other detailed studies of well and seismic data from the Gullfaks Field demonstrate that the vast majority of the (curvi-)linear features are caused by the interference of dipping coherent noise with real reflections (Hesthammer & Fossen 1997*a*, *b*, 1998; Hesthammer & Løkkebø 1997; Hesthammer 1998, 1999*a*). This interference causes the real reflections to break up and rotate in the direction of the dipping noise, thus giving the appearance of a faulted layer. The noise interference features are particularly abundant in areas of poor seismic data quality and along weak seismic reflections. The latter is especially obvious in Figure 5b, which is a timedip map of the Cook Fm. reflection from the same area as shown in Figure 5a. The reflection is associated with weaker amplitudes and, as a result, it is generally not possible to extract detailed structural information from the seismic attribute maps. The reason that the main fault can be observed (the through-going black centerlines) on the timedip map from the Cook Fm. reflection is that the snapping routine uses the subjective interpretation, which is in part based on observations from well log correlation, as a guide and is therefore forced to follow the fault plane. In this sense, the timedip map is only semi-objective. Efforts to image the faults by using fully objective mapping techniques, such as the coherence or correlation maps (Bahorich & Farmer 1995; Brenneke 1995; George 1996), fail when the data quality becomes this poor (Hesthammer 1998). By combining different seismic surveys and applying strong frequency and dip filters to the seismic data, much of the noise features can be removed or diminished (Hesthammer & Løkkebø 1997, Hesthammer 1999*a*).

One of the main motivations for collecting new seismic surveys over the Gullfaks structure in 1995 and 1996 was to explore the potential of time-lapse (4D) seismic. Figure 6 shows amplitude maps of the Tarbert Fm. from the 1985 (Fig. 6a) and 1996 (Fig. 6b) seismic surveys. In addition, Figure 6c displays the differences in amplitude values between the two surveys. There is a marked difference in the seismic amplitudes around injector 34/10–B-12 between the two surveys. In particular, the amplitude map from the 1996 seismic survey displays weaker values near the well. This is likely related to replacement of oil by water due to injection and production. This replacement changes the velocity properties of the rock and therefore the seismic reflectivity.

In 1997, a producer (34/10–C-36) was drilled into the footwall of a domino-style fault block that contains the B-12 injector (i.e. updip of well 34/10–B-12). The well experienced early water breakthrough, consistent with observations from the seismic attribute maps which indicate that the waterfront had almost reached 34/10–C-36 prior to drilling of the well. Unfortunately, processing and analysis of the 4D data were not finished when the C-36 well was planned. As a result, the well was planned and drilled without incorporating results from integrated studies of well data from the 34/10–B-12 well and the two seismic surveys. It is quite possible that the entire cost of the new seismic survey could have been covered by simply placing well 34/10–C-36 more optimally (farther north) based on results from 4D studies.

Well log correlation data

Well 34/10–B-12, which deviates 28° from vertical towards 320 (NW), penetrates reservoir rocks of the Tarbert, Ness, Etive, Rannoch and Cook Fms (Fig. 7). Well log correlation from the area identified two faults in the well. A fault with 69

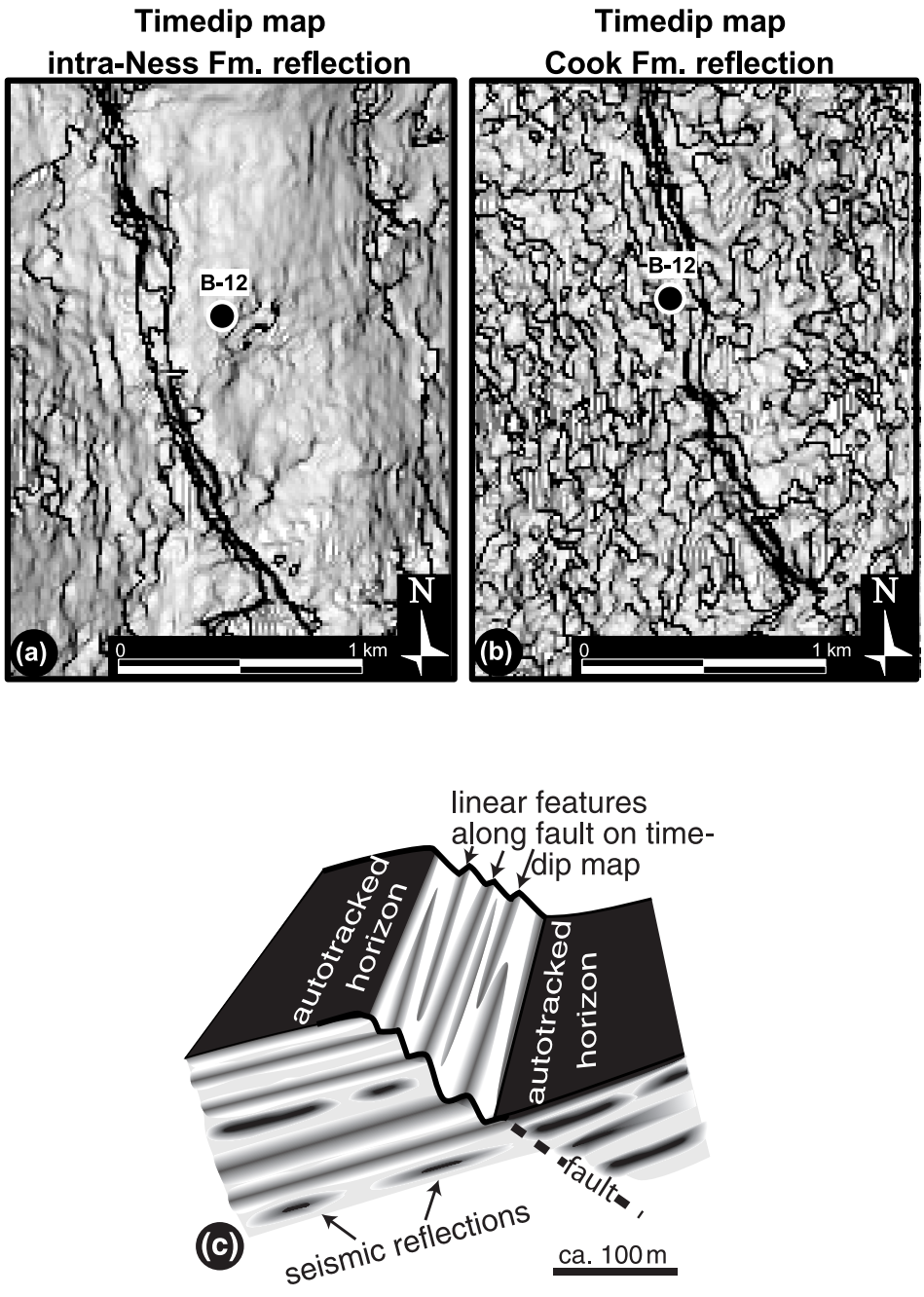

Fig. 5. (**a**) Seismic timedip map of the intra-Ness Fm. reflection in the 1985 seismic survey. The data quality is generally good and the attribute map is little affected by noise. The dark centrelines represent offsets associated with the main faults. (**b**) A timedip map from the Cook Fm. reflection. This seismic reflection is much weaker than the intra-Ness Fm. reflection, and is therefore more affected by (curvi-)linear noise interference features. (**c**) Cartoon illustrating how numerous linear features arise as the autotracked horizon attempts to follow the trace of the fault plane. Where the fault plane reflection is weak or lacking, the autotracked horizon tends to follow bedding plane reflections or multiples in a stepwise manner.

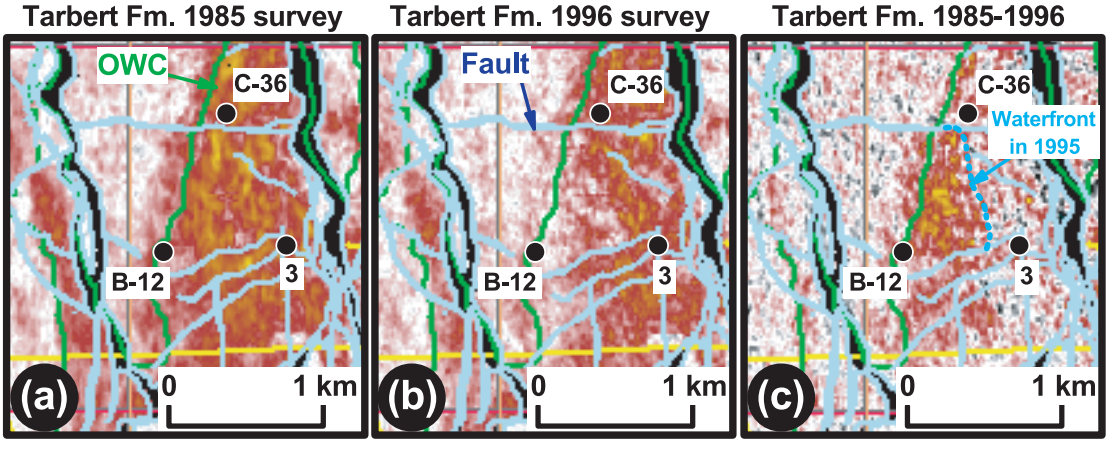

Fig. 6. (**a**) Amplitude map of the Tarbert Fm. from the area around well 34/10–B-12 based on the 1985 seismic survey. (**b**) Amplitude map of the Tarbert Fm. based on the 1996 seismic survey. (**c**) Difference map displaying changes in amplitude values between the two surveys. The changes in reflectivity are likely related to changes in reservoir property caused by injection of water in well 34/10–B-12. The waterfront had almost reached well 34/10–C-36 by the time the C-36 well was drilled and the well experienced water breakthrough shortly after production was initiated. The dark green lines represent the initial oil–water contact.

m missing section is located within the Rannoch Fm. at 2950 m measured depth (MD) (2170 m true vertical depth, TVD) and a fault with 92 m missing section exists in the Drake Fm. at 2983 m MD (2199 m TVD). Due to the large number of wells on the Gullfaks Field, the sedimentologists are generally able to locate minor faults with as little as 4 or 5 m missing section. Furthermore, studies show that more or less all faults on the Gullfaks Field with displacements larger than 10 m are identified from well log correlation (Fossen & Rørnes 1996; Fossen & Hesthammer 2000). The area around well 34/10–B-12 contains several other wells that make detailed control of isopach thickness possible. In particular, correlation against a nearby exploration well (34/10–3) shows that any possible additional faults in well 34/10–B-12 must have displacement less than 3–5 m.

Dipmeter data

Dipmeter data yield information on a scale between seismic data and core data (Rønningsland 1990; Kaya & Norman 1993; Hurley 1994). Well 34/10–B-12 was drilled with oil-based mud. As a result, it was necessary to use an oil-based dipmeter tool to record information on resistivity changes caused by lithological changes (Schlumberger 1986, 1990, 1991; Stuart-Bruges 1984; Dumont *et al*. 1987). Studies from more than 23 km of dipmeter data from the Gullfaks Field demonstrate that, although the data quality from oil-based dipmeter tools is poorer than the quality from water-based tools, it is commonly possible to obtain good control on changes in bedding orientation (Hesthammer & Fossen 1998). Figure 8 shows the results of processing the resistivity curves acquired by the dipmeter tool. In general, the data quality of the resistivity curves indicates good borehole conditions and little tool sticking. However, since the use of oil-based mud causes more scatter of the resulting tadpoles, care must be taken when carrying out structural interpretation.

The general dip of bedding in well 34/10–B-12 changes from 12–14° towards the west in the uppermost parts of the well to subhorizontal and even shallow dips to the east near the faults located at 2950 m MD and 2983 m MD. The gradual decrease in dip of bedding is consistent with observations of large-scale drag towards the east-dipping faults as seen in seismic data (Fig. 4). A sudden change in dip occurs around 2900 m MD. Although this interval contains much scatter, it appears that the dip is much higher than for the intervals above and below. If the change in dip of bedding is caused by drag related to a fault, the fault must dip in a westerly direction since the interval is characterized by steepening drag (Bengtson 1981; Hesthammer & Fossen 1998). The well log correlation, however, shows that no larger faults exist in the interval around 2900 m MD. Any faults must, therefore, have displacement less than 3–5 m. Also, the seismic data show no indications of a westerly

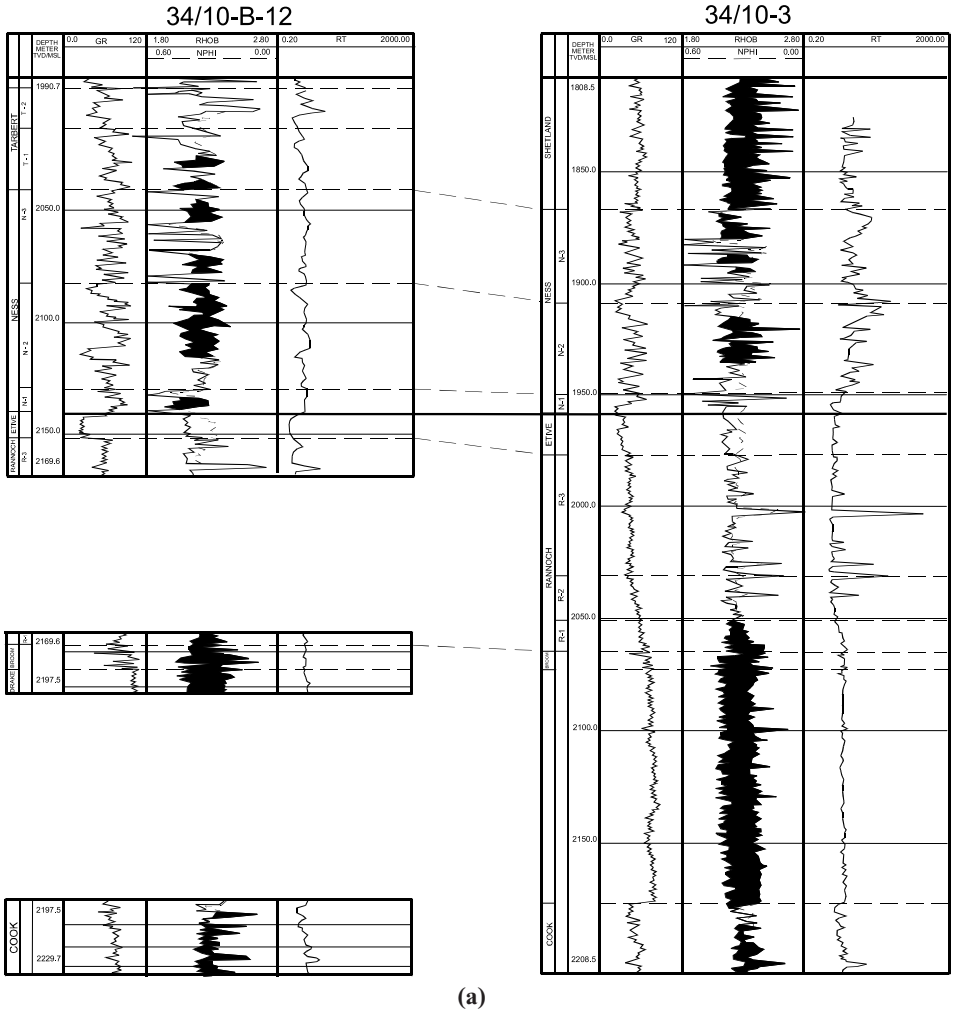

Fig. 7. (**a**) Well log from well 34/10–B-12. See Figure 2 for lithological description. (**b**) Geological profile along well 34/10–B-12.

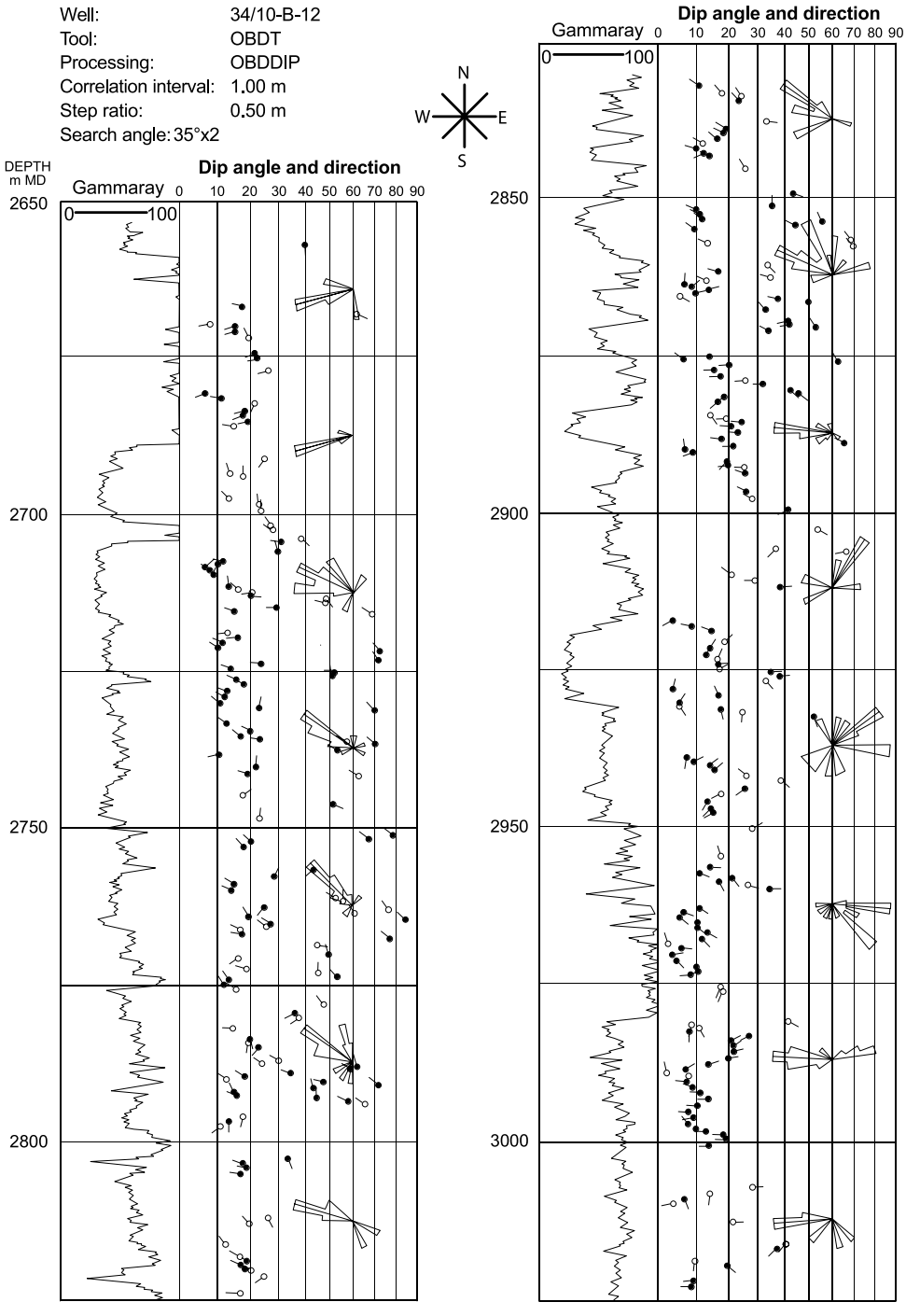

Fig. 8. Dipmeter data from well 34/10–B-12. The well was drilled using oil-based mud. It was therefore necessary to use an oil-based dipmeter tool. This causes more scatter of the processed data than data collected using a water-based dipmeter tool. It is, however, still quite possible to observe general changes in bedding orientation from the oil-based dipmeter data. Dip of bedding decreases with depth and shows easterly dip near the two main faults.

dipping fault, suggesting that any displacement must be below seismic resolution (i.e. 20–30 m). Since there is no obvious relationship between the width of the zone affected by local drag of bedding and the displacement of the faults on the Gullfaks Field, it is quite possible that a minor antithetic fault is located around 2900 m MD.

In the interval from 2950 to 2985 m MD, where the two large-scale faults are located, many of the dipmeter measurements indicate easterly dip. Seismic data clearly demonstrate that the faults must dip in an easterly direction. This suggests that the two faults are associated with flattening drag and that bedding decreases from 12–14° towards the west in the Tarbert Fm. to subhorizontal and easterly dip in the Rannoch and Drake Fms. Dipmeter data alone are not of sufficiently good quality that detailed changes in bedding orientation can be observed, and such data must therefore be used in conjunction with other data types.

The amount of dip of the two faults cannot be determined with certainty from dipmeter data alone. It may, however, be possible to indicate a rough minimum dip of the faults by identifying the maximum dip of the strata at the exact location of the faults. Only if bedding is dragged completely parallel to the faults can studies of bedding dip give the exact dip of the faults. At the location of the faults, there are indications of localized drag, suggesting easterly fault dips in excess of 20–40°. Since the data are processed from an oil-based dipmeter tool, such detailed interpretation must be treated with extreme care and should not be used alone. In the present case, seismic data (Fig. 4) indicate that the faults dip approximately 25–35° towards the east, which is consistent with observations from dipmeter data.

Core data

Core data provide the geologist with the most detailed information about reservoir properties. The reservoir rocks in the hanging wall to the main faults were cored in well 34/10–B-12 to investigate petrophysical, sedimentological and structural properties. Figure 9a displays the frequency of deformation bands per half metre as observed from cores in well 34/10–B-12. Deformation bands are microfaults with less than a few centimetres of displacement. In addition, the bands have not developed distinct slip surfaces and, therefore, represent localized areas of strain hardening rather than the typical weakening of rocks associated with larger-scale faults (e.g. Antonellini *et al*. 1994). It is clear from the diagram that the two main faults located at 2950 m MD and 2983 m MD are associated with abundant deformation bands in a narrow interval that defines the width of the deformation zones. In addition, there is an interval of abundant deformation bands located around 2900 m MD. This is the same location where dip of bedding increased according to dipmeter data. Well log correlation data demonstrate that a possible fault can only be associated with minor (3–5 m) displacement. The width of the damage zone for the possible minor fault located at 2900 m MD is wider than that observed around the 69 m fault located at 2950 m MD. This observation may be surprising, but is consistent with other studies of core data from the Gullfaks Field, which show no simple relationship between the width of a fault's damage zone and the displacement of the fault (Hesthammer & Fossen 2001). The reason for this may be that the deformation bands were created prior to development of a distinct slip surface (Aydin & Johnson 1978, 1983; Fossen & Hesthammer 1998*b*). Once a weak slip surface exists, there is no need to develop more deformation bands unless irregular fault plane geometries cause local areas of fault locking and strain hardening.

A total of 256 m of cores exist for the B-12 well. Of these, 222.6 m were available for analyses. The remaining interval was either missing (6.9 m), characterized by low coherence (22.2 m) or intensely tectonically fragmented (4.3 m). A total of 392 deformation bands were identified, most of which occur in narrow damage zones. The average displacement along each deformation band is 6.1 mm. This gives an accumulated displacement for all deformation bands in the well of 2.4 m. This is much too little to explain the gradual decrease of bedding observed in the hanging wall (large-scale drag) as being caused by deformation bands alone. In addition, well log correlation and dipmeter data demonstrate that there are not enough faults with discrete slip surfaces to account for the change in bedding dip. Since deformation of the Gullfaks Field occurred immediately after deposition of the Brent Group when the sediments were only loosely consolidated, it is likely that much of the sub-seismic deformation occurred by a reorganization of individual grains rather than by discrete fractures or deformation bands (Hesthammer 1999*b*).

Figure 9b shows dip of bedding with respect to depth as observed from core data. Since the well is deviated from vertical, the measurements do not represent the true dip of bedding. The observed gradual decrease in bedding dip towards the two main faults supports observations of hanging wall drag from seismic and dipmeter data. In addition, the high dip of

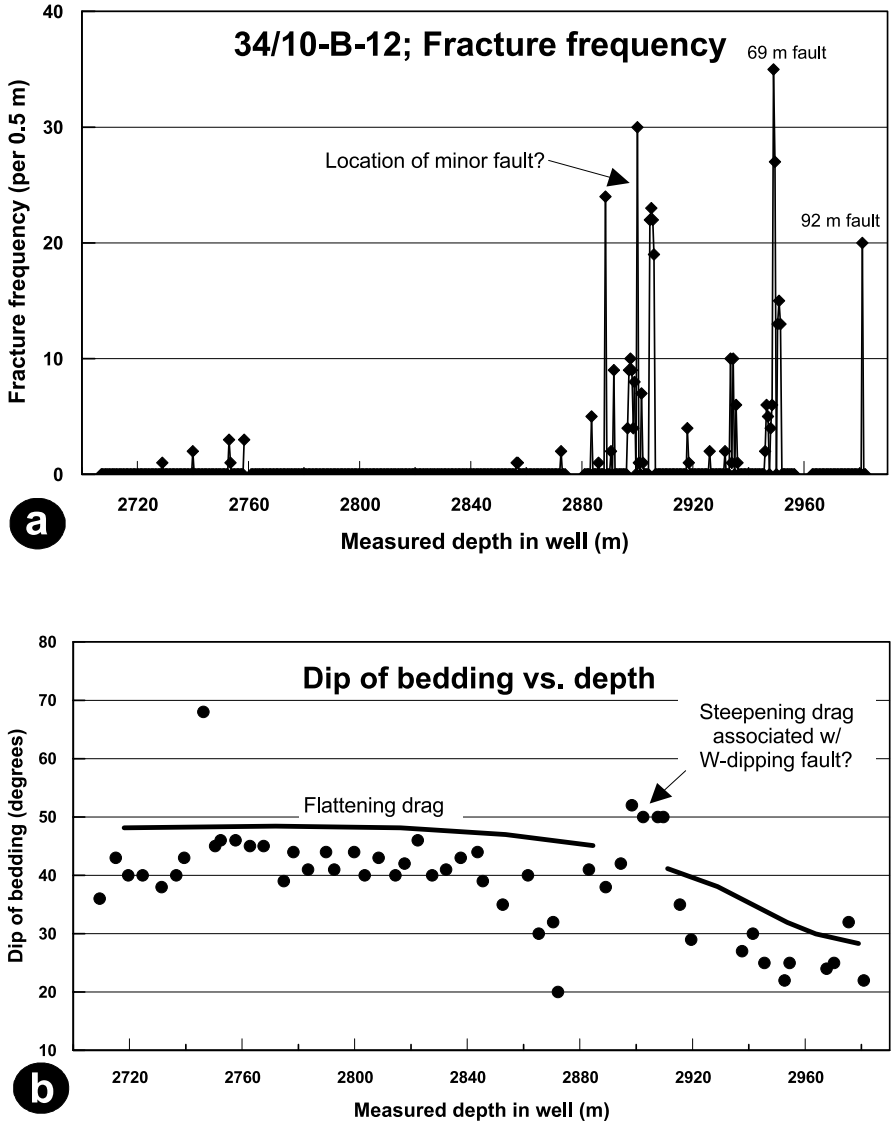

Fig. 9. (**a**) Fracture frequency diagram for well 34/10–B-12. Number of deformation bands per half metre is plotted along the y-axis whereas measured depth is plotted along the x-axis. The two faults associated with 69 m and 92 m missing section in the Rannoch and Drake Fms, respectively, are associated with a narrow deformation zone containing numerous deformation bands. Also, a minor fault (less than 3–5 m offset) may be located around 2900 m MD where another cluster of deformation bands is observed. (**b**) A plot showing change in dip (as observed in core data) versus depth illustrates how the dip of bedding decreases towards the main faults. This is a result of large-scale drag in the hanging wall. A steepening drag associated with a minor fault may be observed at around 2900 m MD. Modified after Hesthammer & Henden (2000).

bedding observed from dipmeter data around 2900 m MD is also clearly observed in the core data. This supports the view that a westerly dipping fault with minor offset is located within this interval.

The core from well 34/10–B-12 was not orientated. It is, therefore, not possible from core data alone to determine the exact bedding orientation. However, observations of dip from the slabbed core (the core is slabbed parallel to

the dip direction of bedding) allows calculations of a solution population curve showing all possibilities for bedding orientation (see Hesthammer (1998) for a description of the procedure). Figure 10 shows solution population curves for bedding orientation for the Tarbert Fm. (blue curve), Ness Fm. (green curve), Etive Fm. (yellow curve), Rannoch Fm. (orange curve) and the Drake Fm. (red curve). Seismic data from the Tarbert Fm. indicate a dip of 13° towards 290. This is consistent with observations from dipmeter data. Also, the interpreted orientation from dipmeter and seismic data plot on the solution population curve from core data. This gives a unique orientation of bedding for the Tarbert Fm. Similarly, seismic interpretation of the intra-Ness Fm. reflection indicates that bedding dips 6° towards 295, which is also consistent with observations from dipmeter data. These measurements plot on the solution population curve for bedding orientation measured from core data from the Ness Fm.

Although seismic data and dipmeter data are not conclusive for measurements of bedding orientation within the Etive Fm., core data suggest that bedding dip is subhorizontal. Within the Rannoch and Drake Fms, dipmeter data and core data both suggest that the bedding dips shallowly (2–4°) towards the east.

These observations are consistent with large-scale drag related to a ESE-dipping fault. The 69 m fault located at 2950 m MD is associated with a zone of fault breccia (Fig. 11). Abundant deformation bands appear to be subparallel to the edges of the brecciated zone. It is thus likely that the deformation bands are subparallel to the large-scale fault. Since bedding orientation is determined from seismic, dipmeter and core data, it is possible to estimate the orientation of the deformation bands and faults as observed in the core data and thus estimate the orientation of any larger-scale fault. There are two different approaches that may be applied. One is to use vector calculations and polar coordinates, as described by Hesthammer & Henden (2000).

A different approach is to use stereographic projection. This method does not require the use of mathematics and is easier if only a few orientation data are to be measured. The well is deviated 28° from vertical towards 320, indicated

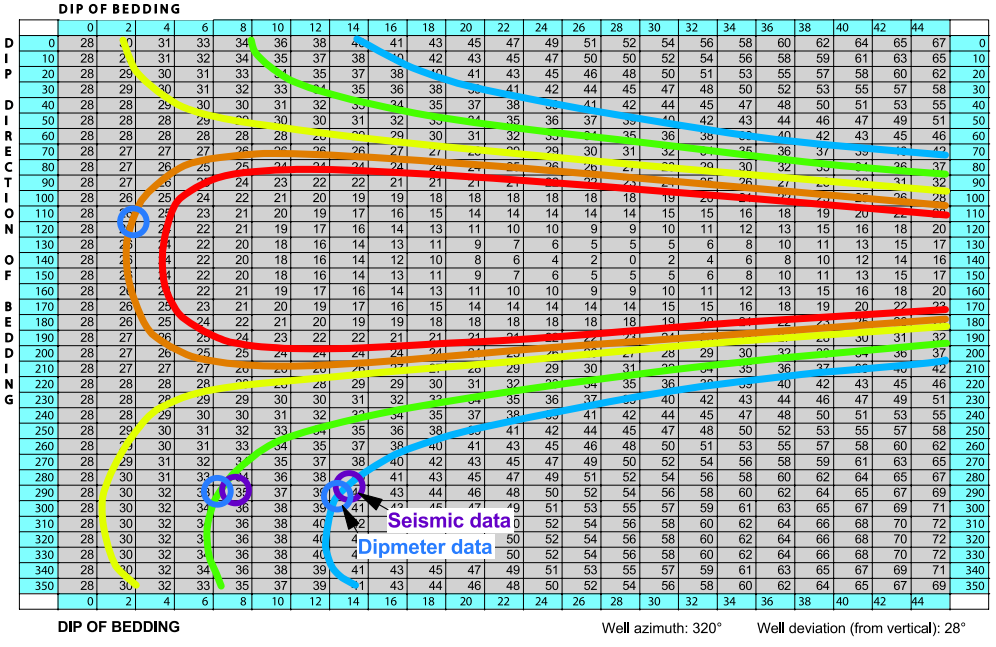

Fig. 10. Solution population diagram for possible orientations of bedding based on analyses of core data from well 34/10–B-12. The dip of bedding decreases from 12–14° towards the west in the Tarbert Fm. (blue curve) to 6° in the Ness Fm. (green curve), via subhorizontal in the Etive Fm. (yellow curve) to easterly dips in the Rannoch and Drake Fms (orange and red curves, respectively). Seismic data and dipmeter data are consistent with core data, thus verifying the gradual change in bedding dip.

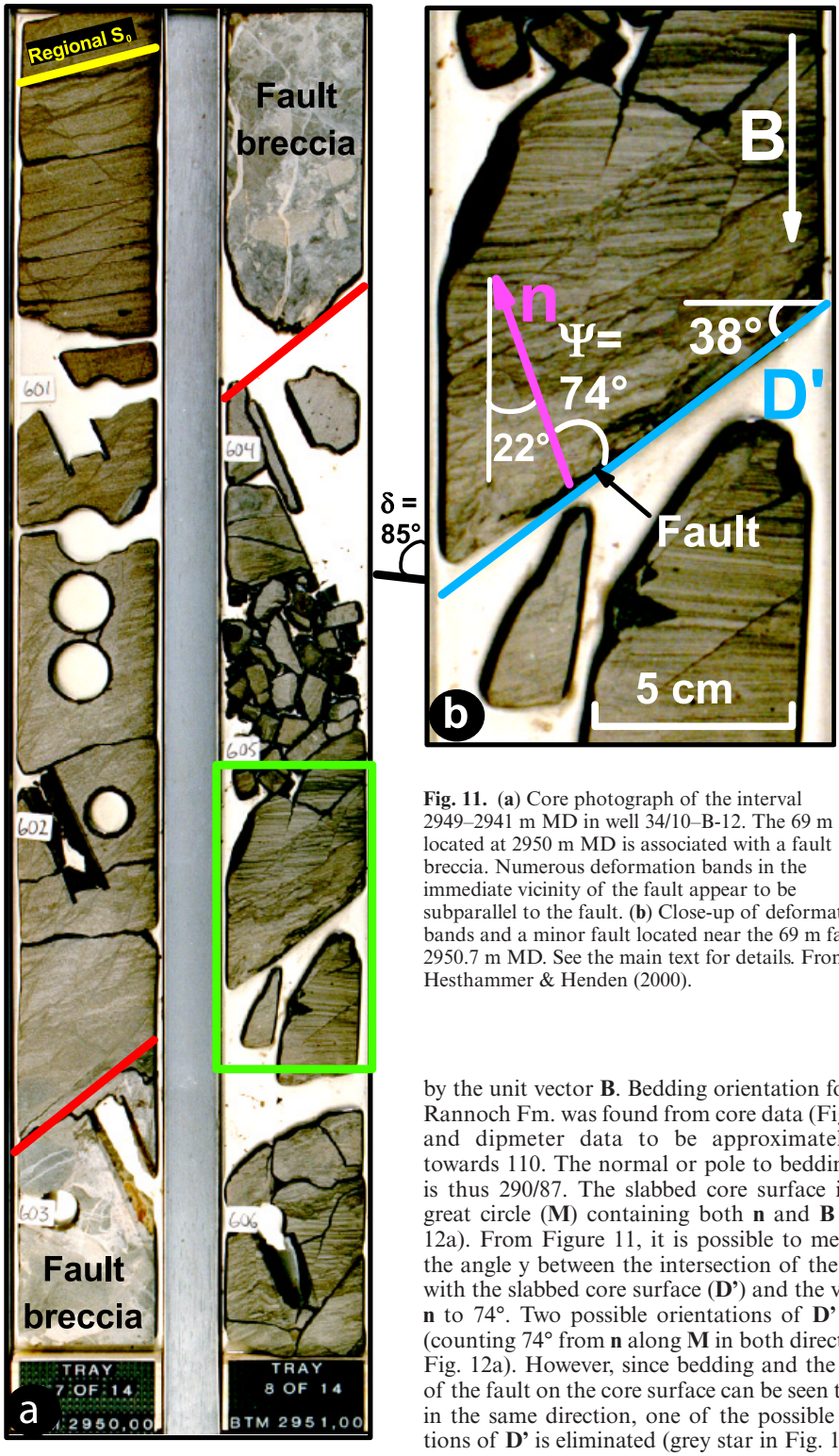

Fig. 11. (**a**) Core photograph of the interval 2949–2941 m MD in well 34/10–B-12. The 69 m fault located at 2950 m MD is associated with a fault breccia. Numerous deformation bands in the immediate vicinity of the fault appear to be subparallel to the fault. (**b**) Close-up of deformation bands and a minor fault located near the 69 m fault at 2950.7 m MD. See the main text for details. From Hesthammer & Henden (2000).

by the unit vector **B**. Bedding orientation for the Rannoch Fm. was found from core data (Fig. 10) and dipmeter data to be approximately 3° towards 110. The normal or pole to bedding (**n**) is thus 290/87. The slabbed core surface is the great circle (**M**) containing both **n** and **B** (Fig. 12a). From Figure 11, it is possible to measure the angle y between the intersection of the fault with the slabbed core surface (**D'**) and the vector **n** to 74°. Two possible orientations of **D'** arise (counting 74° from **n** along **M** in both directions; Fig. 12a). However, since bedding and the trace of the fault on the core surface can be seen to dip in the same direction, one of the possible positions of **D'** is eliminated (grey star in Fig. 12a).

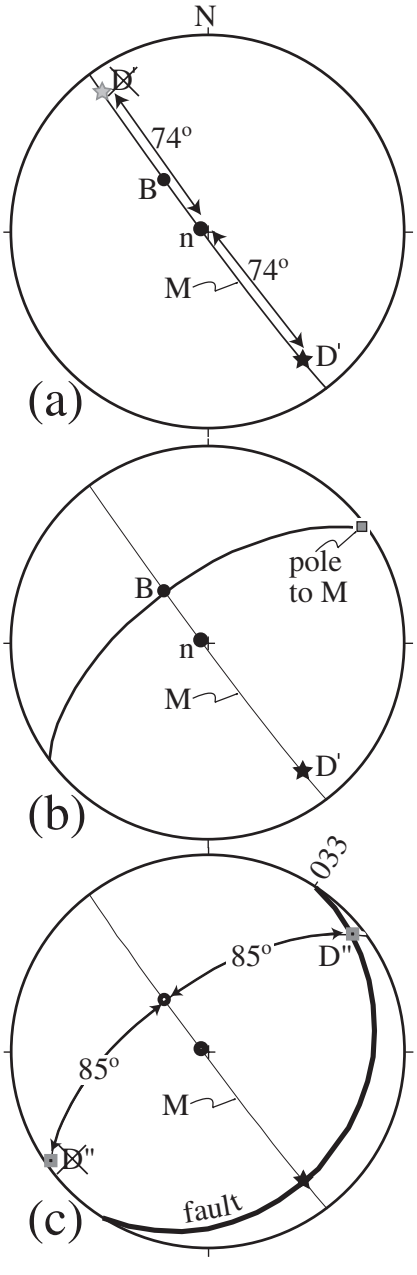

Fig. 12. Stereographic projection showing the unique solution of fault orientation for the 69 m fault located at 2950 m MD in well 34/10–B-12. The diagram shows that the fault must dip 21° towards 123 (SE). This is consistent with observations from dipmeter data and seismic data. M is the slabbed core surface displayed in Figure 11, **n** is the pole to bedding, **D'** is the trace of the fault on **M**, and **D"** is the corresponding trace on the core section perpendicular to **M**. See text for further explanation.

Plotting the pole to **M** and drawing a great circle through this pole and **B** displays the section perpendicular to the main slabbed core surface (Fig. 12b). The trace of the fault (**D"**) in this section makes an acute angle (d) of 85° with **B**. Since the angle can be measured in both directions along the great circle, we are left with two possibilities for **D"** (Fig. 12c). We observe the direction of apparent dip of layering (and **D'**) in the M-section is to the left (Fig. 11). From the stereonet data this means that we are looking at the M-surface from the NE. Knowing from core observation that **D"** is plunging out of the page (Fig. 11), i.e. to the NE, enables us to choose the NE-plunging alternative for **D"** (Fig. 12c). The great circle that contain **D"** and **D'** represents the fault, which is dipping about 21° towards 123 (SE). This result is consistent with observations from seismic data (Figs 3 & 4) and dipmeter data (Fig. 8) and demonstrates how analyses of different data types can be integrated to obtain a coherent structural interpretation.

A similar approach can be applied to the fault located at 2983 m MD. The fault itself is not preserved within the cored section and it is necessary to assume that the nearby deformation bands are subparallel to the fault. Figure 13 shows a core photograph near the fault. Values of y and d from the intersection of a deformation band with the slabbed core surface and the section orientated perpendicular to this were measured to 64° and 100°, respectively. Orientation of bedding was measured from dipmeter data and core data to be 5° towards 110 within the Drake Fm. The well orientation is the same as within the Rannoch Fm. The resulting unique solution based on stereographic projection (Fig. 14) shows that the fault must dip 33° towards 124. This is sufficiently close to the orientation of the fault located at 2950 m MD to assume that they are subparallel, as is indeed indicated by seismic data and dipmeter data.

Conclusions

Integrated, rather than individual, analyses of all available data enable the structural interpreter to confidently understand the characteristics of reservoir geometries. Typical data types that are available for structural interpretation include seismic, well log correlation, dipmeter and core data. The range in scale varies from many kilometres to less than a millimetre. Since the different data types normally overlap in scale, it is possible to control the quality results from the analyses and thereby strengthen the observations or identify possible sources of error.

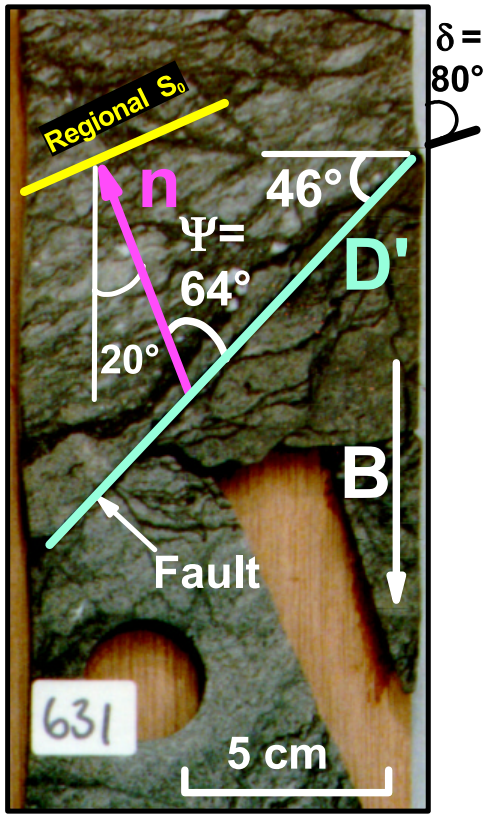

Fig. 13. Core photograph near the 92 m fault located at 2983 m MD in well 34/10–B-12. Several deformation bands are identified. See the main text for detailed discussion. From Hesthammer & Henden (2000).

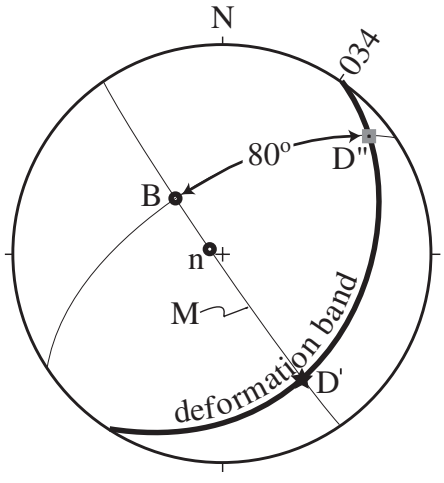

Fig. 14. Stereographic projection showing the orientation of the deformation band located near the 92 m fault at 2983 m MD in well 34/10–B-12. Analyses of core data show that the fault likely dips 33° towards 124 (ESE). This is subparallel to the 69 m fault located at 2950 m MD and consistent with observations from dipmeter data and seismic data. See text for further explanation.

Integrated use of seismic and well data from the area around well 34/10–B-12 on the Gullfaks Field has helped the structural geologist to understand the properties and geometries of the reservoir. In particular, the data analyses lead to the following conclusions:

Seismic data are of reasonably good quality in the area around the B-12 well and show that at least one large-scale east-dipping fault cut through the seismic reflections. The fault is associated with hanging-wall drag, which affects most of the reservoir penetrated by well 34/10–B-12.

Studies of time-lapse seismic identify a waterfront caused by injection of water in well 34/10–B-12. This waterfront was verified by water breakthrough in well 34/10–C-36 located updip of the B-12 well.

Well log correlation identified two large-scale faults located only a few metres apart: a fault associated with 69 m missing section within the Rannoch Fm. and a fault with 92 m missing section in the Drake Fm. Any additional faults must have displacements less than 3–5 m.

Dipmeter data show that the dip of bedding in the 34/10–B-12 well decreases from 12–14° at the uppermost reservoir level to subhorizontal and shallow easterly dip in the lowermost parts of the well. The two large-scale faults are associated with easterly dip of bedding and flattening drag, suggesting that the faults must dip to the east. This is consistent with observations from seismic data.

Core data demonstrate that the two large-scale faults are associated with abundant deformation bands in a narrow deformation zone. The number of deformation bands is too small to account for the change in bedding dip associated with the large-scale drag in the hanging wall. Since well log correlation shows that no larger fault exists in the hanging wall to the main faults, it is likely that most of the deformation was by a widely distributed grain reorganization rather than by faulting.

Core data also show that the dip of bedding decreases towards deeper reservoir levels. Bedding orientation measurements from seismic data and dipmeter data plot on the solution population curves for possible bedding orientation based on core data. This verifies that the different data types are consistent and reliable.

Analyses of fault orientation from core data show that the 69 m fault located at 2950 m MD must dip 23° towards 120, whereas the 92 m fault located at 2983 m MD dip 32° towards 125. This is consistent with observations of fault orientation from seismic data and dipmeter data.

The authors would like to thank Statoil and Norsk Hydro for permission to publish this paper.

References

Antonellini, M., Aydin, A. & Pollard, D. D. 1994. Microstructure of deformation bands in porous sandstones at Arches National Park, Utah. *Journal of Structural Geology,* **16**, 941–959.

Aydin, A. & Johnson, A. M. 1978. Development of faults as zones of deformation bands and as slip surfaces in sandstones. *Pure and Applied Geophysics,* **116**, 931–942.

Aydin, A. & Johnson, A. M. 1983. Analysis of faulting in porous sandstones. *Journal of Structural Geology,* **5**, 19–31.

Bahorich, M. & Farmer, S. 1995. 3–D seismic discontinuity for faults and stratigraphic features: the coherence cube. *Leading Edge,* **14**, 1053–1058.

Bengtson, C. A. 1981. Statistical curvature analysis techniques for structural interpretation of dipmeter data. *AAPG Bulletin* **65**, 312–332.

Brenneke, J. C. 1995. Analysis of fault traps. *World Oil,* **216**, 63–71.

Dalley, R. M., Gevers, E. C. A., Stampfli, G. M., Davies, D. J., Gastaldi, C. N., Ruijtenberg, P. A. & Vermeer, G. J. O. 1989. Dip and azimuth displays for 3D seismic interpretation. *First Break,* **7**, 86–95.

Dumont, A., Kubacsi, M. & Chardac, J. L. 1987. The oil-based mud dipmeter tool. *28th Annual SPWLA Logging Symposium,* **2**.

Fossen, H. & Hesthammer, J. 1998*a*. Structural geology of the Gullfaks Field. *In*: Coward, M. P., Johnson, H & Daltaban, T. S. (eds) *Structural Geology in Reservoir Characterization*. Geological Society, London, Special Publications, **127**, 231–261.

Fossen, H. & Hesthammer, J. 1998*b*. Deformation bands and their significance in porous sandstone reservoirs. *First Break,* **16**, 21–25.

Fossen, H. & Hesthammer, J. 2000. Possible absence of small faults in the Gullfaks Field, northern North Sea: implications for downscaling of faults in some porous sandstones. *Journal of Structural Geology* **22**, 851–863.

Fossen, H. & Rørnes, A. 1996. Properties of fault populations in the Gullfaks Field, northern North Sea. *Journal of Structural Geology,* **18**, 179–190.

George, D. 1996. Coherence cube reveals stratigraphic features more readily than traditional 3D seismic slice plots. *Offshore International,* **56**, 22–23.

Hesthammer, J. 1998. Integrated use of well data for structural interpretation of seismic data. *Petroleum Geoscience,* **4**, 97–109.

Hesthammer, J. 1999*a*. Improving seismic data for detailed structural interpretation. *The Leading Edge*, **18**, 226–247.

Hesthammer, J. 1999b. *Analysis of fault geometry and internal fault block deformation in the Gullfaks region, northern North Sea*. PhD thesis, University of Bergen, Norway.

Hesthammer, J. & Fossen, H. 1997*a*. Seismic attribute analysis in structural interpretation of the Gullfaks Field, northern North Sea. *Petroleum Geoscience,* **3**, 13–26.

Hesthammer, J. & Fossen, H. 1997*b*. The influence of seismic noise in structural interpretation of seismic attribute maps. *First Break,* **15**, 209–219.

Hesthammer, J. & Fossen, H. 1998. The use of dipmeter data to constrain the structural geology of the Gullfaks Field, northern North Sea. *Marine and Petroleum Geology,* **15**, 549–573.

Hesthammer, J. Landrø, M. & Fossen, H. 2001. Use and abuse of seismic data in reservoir characterisation. *Marine and Petroleum Geology,* **18**, 635–655.

Hesthammer, J., & Fossen, H. 2001. Structural core analysis from the Gullfaks area, northern North Sea. *Marine and Petroleum Geology,* **18**, 411–439.

Hesthammer, J. & Henden, J. O. 2000. Information on fault orientation from unoriented cores. *AAPG Bulletin*, **84**, 472–488.

Hesthammer, J. & Løkkebø, S. M. 1997. Combining seismic surveys to improve data quality. *First Break,* **15**, 103–115.

Hoetz, H. L .J. G. & Watters, D. G. 1992. Seismic horizon attribute mapping for the Annerveen Gasfield, the Netherlands. *First Break,* **10**, 41–51.

Hurley, N. F. 1994. Recognition of faults, unconformities, and sequence boundaries using cumulative dip plots. *AAPG Bulletin* **78**, 1173–1185.

Kaya, M. A. & Norman, T. N. (1993) Verifying a geological structure by applying SCAT (statistical curvarure analysis techniques) method on dipmeter data at the Umurca Field in the Turkish Thrace. *4th Annual SPE and Archie Conference Proceedings*, 67–72.

Rønningsland, T. M. 1990. Structural interpretation of dipmeter results in the Gullfaks Field. *In*: Hurst, A., Lovell, M. A. & Morton, A. C. (eds) *Geological Applications of Wireline Logs*. Geological Society Special Publications, London **48**, 273–286.

Schlumberger 1986. *Dipmeter Interpretation*. Schlumberger Limited, Texas.

Schlumberger 1990. *Data Services Catalog*. Schlumberger Educational Services, New York.

Schlumberger 1991. *Wireline Services Catalog.* Schlumberger Educational Services, Texas.

Stuart-Bruges, W. P. 1984. A dipmeter for use in oil based muds. *9th International SAID (division of SPWLA) Formation Evaluation Symposium*.

Tollefsen, S., Graue, E. & Svindal, S. 1994. Gullfaks development provides challenges. *World Oil* (April), 45–54.

Voggenreiter, W. R. 1991. Kapuni 3D interpretation – imaging Eocene paleogeography. *New Zealand Oil Exploration Conference Proceedings,* **1**, 287–298.